THE JOURNAL OF PHYSICAL CHEMISTRY Letters

pubs.acs.org/JPCL Letter

Pros and Cons of the Bethe–Salpeter Formalism for Ground-State Energies

Pierre-François Loos,* Anthony Scemama, Ivan Duchemin, Denis Jacquemin,* and Xavier Blase*

Cite This: J. Phys. Chem. Lett. 2020, 11, 3536–3545 Read Online

ACCESS | Metrics & More | Article Recommendations | Supporting Information

ABSTRACT: The combination of the many-body Green's function *GW* approximation and the Bethe–Salpeter equation (BSE) formalism has shown to be a promising alternative to time-dependent density functional theory (TD-DFT) for computing vertical transition energies and oscillator strengths in molecular systems. The BSE formalism can also be employed to compute ground-state correlation energies thanks to the adiabatic-connection fluctuation–dissipation theorem (ACFDT). Here, we study the topology of the ground-state potential energy surfaces (PESs) of several diatomic molecules near their equilibrium bond length. Using comparisons with state-of-art computational approaches (CC3), we show that ACFDT@BSE is surprisingly accurate and can even compete with lower-order coupled cluster methods (CC2 and CCSD) in terms of total energies and equilibrium bond distances for the considered systems. However, we sometimes observe unphysical irregularities on the ground-state PES in relation with difficulties in the identification of a few *GW* quasiparticle energies.

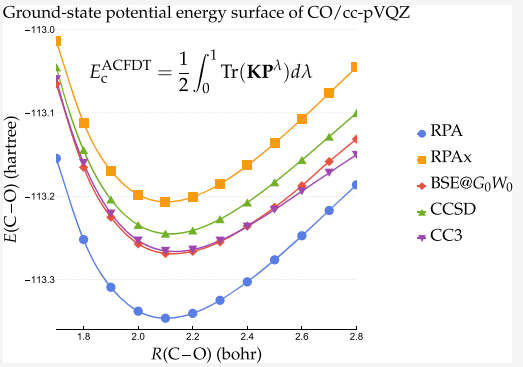

With a similar computational scaling as time-dependent density-functional theory (TD-DFT),[1,2] the many-body Green's function Bethe–Salpeter equation (BSE) formalism[3−8] is a valuable alternative that has gained momentum in the past few years for studying molecular systems.[9−21] It now stands as a cost-effective computational method that can model excited states[22,23] with a typical error of 0.1–0.3 eV for spin-conserving transitions according to large and systematic benchmarks.[24−30] One of the main advantages of BSE compared to TD-DFT is that it allows a faithful description of charge-transfer states.[31−36] Moreover, when performed on top of a (partially) self-consistent ev*GW* calculation,[37−43] BSE@ev*GW* has been shown to be weakly dependent on its starting point (*e.g.*, on the exchange–correlation functional selected for the underlying DFT calculation).[24,43] However, similar to adiabatic TD-DFT,[44−47] the static version of BSE cannot describe multiple excitations.[48−50]

A significant limitation of the BSE formalism, as compared to TD-DFT, lies in the lack of analytical nuclear gradients (*i.e.*, the first derivatives of the energy with respect to the nuclear displacements) for both the ground and excited states,[51] preventing efficient studies of excited-state processes (*e.g.*, chemoluminescence and fluorescence) associated with geometric relaxation of ground and excited states and structural changes upon electronic excitation.[52−55] While calculations of the *GW* quasiparticle energy ionic gradients are becoming increasingly popular,[56−61] only one pioneering study of the excited-state BSE gradients has been published to date.[62] In this seminal work devoted to small molecules (CO and NH_3), only the BSE excitation energy gradients were calculated while computing the Kohn–Sham (KS) LDA forces as its ground-state contribution.

In contrast to TD-DFT which relies on KS-DFT[63−65] as its ground-state analogue, the ground-state BSE energy is not a well-defined quantity, and no clear consensus has been found regarding its formal definition. Consequently, the BSE ground-state formalism remains in its infancy with very few available studies for atomic and molecular systems.[66−69] In the largest available benchmark study[67] encompassing the total energies of the atoms H–Ne, the atomization energies of the 26 small molecules forming the HEAT test set,[70] and the bond lengths and harmonic vibrational frequencies of 3d transition-metal monoxides, the BSE correlation energy, as evaluated within the adiabatic-connection fluctuation–dissipation theorem (ACFDT) framework,[71] was mostly discarded from the set of tested techniques because of instabilities (negative frequency modes in the BSE polarization propagator) and replaced by an approximate (RPAsX) approach where the screened-Coulomb potential matrix elements were removed from the resonant electron–hole contribution.[67,72] Such a modified BSE polarization propagator was inspired by a previous study on the homogeneous electron gas (HEG).[72]

Received: February 11, 2020
Accepted: April 16, 2020
Published: April 16, 2020

https://dx.doi.org/10.1021/acs.jpclett.0c00460
J. Phys. Chem. Lett. 2020, 11, 3536–3545

Within RPAsX, amounting to neglecting excitonic effects in the electron−hole propagator, the question of using either KS-DFT or *GW* eigenvalues in the construction of the propagator becomes more relevant, increasing accordingly the number of possible definitions for the ground-state correlation energy. Finally, renormalizing or not the Coulomb interaction by the interaction strength λ in the Dyson equation for the interacting polarizability (see below) leads to two different versions of the BSE correlation energy,[67] emphasizing further the lack of general agreement around the definition of the ground-state BSE energy.

Here, in analogy to the random-phase approximation (RPA)-type formalisms[73−77] and similarly to refs 66, 67, and 72, the ground-state BSE energy is calculated in the adiabatic connection framework. Embracing this definition, the purpose of the present Letter is to investigate the quality of ground-state PES near equilibrium obtained within the BSE approach for several diatomic molecules. The location of the minimum on the ground-state PES is of particular interest. This study is a first necessary step toward the development of analytical nuclear gradients within the BSE@*GW* formalism. Using comparisons with both similar and state-of-art computational approaches, we show that the ACFDT@BSE@*GW* approach is surprisingly accurate and can even compete with high-order coupled cluster (CC) methods in terms of absolute energies and equilibrium distances. However, we also observe, in some cases, unphysical irregularities on the ground-state PES, which are due to the appearance of a satellite resonance with a weight similar to that of the *GW* quasiparticle peak.[78−82]

In order to compute the neutral (optical) excitations of the system and their associated oscillator strengths, the BSE expresses the two-body propagator[4,83]

$$L(1,2,1',2') = L_0(1,2,1',2') + \int \mathrm{d}3\,\mathrm{d}4\,\mathrm{d}5\,\mathrm{d}6\, L_0(1,4,1',3)\Xi(3,5,4,6)L(6,2,5,2') \tag{1}$$

as the linear response of the one-body Green's function G with respect to a general nonlocal external potential

$$\Xi(3,5,4,6) = i\frac{\delta[v_{\mathrm{H}}(3)\delta(3,4) + \Sigma_{\mathrm{xc}}(3,4)]}{\delta G(6,5)} \tag{2}$$

which takes into account the self-consistent variation of the Hartree potential

$$v_{\mathrm{H}}(1) = -i\int \mathrm{d}2\, v(1,2)\, G(2,2^+) \tag{3}$$

(where v is the bare Coulomb operator) and the exchange−correlation self-energy Σ_{xc}. In eq 1, $L_0(1,2,1',2') = -iG(1,2')\,G(2,1')$, and $(1) = (\mathbf{r}_1, \sigma_1, t_1)$ is a composite index gathering space, spin, and time variables. In the *GW* approximation,[83−87] we have

$$\Sigma_{\mathrm{xc}}^{\mathrm{GW}}(1,2) = iG(1,2)\,W(1^+,2) \tag{4}$$

where W is the screened Coulomb operator, and hence, the BSE reduces to

$$\Xi(3,5,4,6) = \delta(3,4)\delta(5,6)v(3,6) - \delta(3,6)\delta(4,5)W(3,4) \tag{5}$$

where, as commonly done, we have neglected the term $\delta W/\delta G$ in the functional derivative of the self-energy.[88−90] Finally, the static approximation is enforced, *i.e.*, $W(1,2) = W(\{\mathbf{r}_1, \sigma_1, t_1\}, \{\mathbf{r}_2, \sigma_2, t_2\})\delta(t_1 - t_2)$, which corresponds to restricting W to its static limit, *i.e.*, $W(1,2) = W(\{\mathbf{r}_1, \sigma_1\},\{\mathbf{r}_2, \sigma_2\}; \omega = 0)$.

For a closed-shell system in a finite basis, to compute the singlet BSE excitation energies (within the static approximation) of the physical system (*i.e.*, $\lambda = 1$), one must solve the following linear response problem[2,83,91]

$$\begin{pmatrix} \mathbf{A}^\lambda & \mathbf{B}^\lambda \\ -\mathbf{B}^\lambda & -\mathbf{A}^\lambda \end{pmatrix}\begin{pmatrix} \mathbf{X}_m^\lambda \\ \mathbf{Y}_m^\lambda \end{pmatrix} = \Omega_m^\lambda \begin{pmatrix} \mathbf{X}_m^\lambda \\ \mathbf{Y}_m^\lambda \end{pmatrix} \tag{6}$$

where Ω_m^λ is the mth excitation energy with eigenvector $(\mathbf{X}_m^\lambda\ \mathbf{Y}_m^\lambda)^{\mathrm{T}}$ at interaction strength λ; $^{\mathrm{T}}$ indicates the matrix transpose, and we assume real-valued spatial orbitals $\{\phi_p(\mathbf{r})\}_{1\le p\le N}$. The matrices $\mathbf{A}^\lambda$, $\mathbf{B}^\lambda$, $\mathbf{X}^\lambda$, and $\mathbf{Y}^\lambda$ are all of size $OV \times OV$ where O and V are the number of occupied and virtual orbitals (*i.e.*, $N = O + V$ is the total number of spatial orbitals), respectively. In the following, the index m labels the OV single excitations; i and j are occupied orbitals; a and b are unoccupied orbitals, while p, q, r, and s indicate arbitrary orbitals.

In the absence of instabilities (*i.e.*, when $\mathbf{A}^\lambda - \mathbf{B}^\lambda$ is positive-definite),[91] eq 6 is usually transformed into an Hermitian eigenvalue problem of smaller dimension

$$(\mathbf{A}^\lambda - \mathbf{B}^\lambda)^{1/2}(\mathbf{A}^\lambda + \mathbf{B}^\lambda)(\mathbf{A}^\lambda - \mathbf{B}^\lambda)^{1/2}\mathbf{Z}_m^\lambda = (\Omega_m^\lambda)^2\mathbf{Z}_m^\lambda \tag{7}$$

where the excitation amplitudes are

$$(\mathbf{X}^\lambda + \mathbf{Y}^\lambda)_m = (\Omega_m^\lambda)^{-1/2}(\mathbf{A}^\lambda - \mathbf{B}^\lambda)^{+1/2}\mathbf{Z}_m^\lambda \tag{8a}$$

$$(\mathbf{X}^\lambda - \mathbf{Y}^\lambda)_m = (\Omega_m^\lambda)^{+1/2}(\mathbf{A}^\lambda - \mathbf{B}^\lambda)^{-1/2}\mathbf{Z}_m^\lambda \tag{8b}$$

Introducing the so-called Mulliken notation for the bare two-electron integrals

$$(pq|rs) = \iint \frac{\phi_p(\mathbf{r})\phi_q(\mathbf{r})\phi_r(\mathbf{r}')\phi_s(\mathbf{r}')}{|\mathbf{r} - \mathbf{r}'|}\mathrm{d}\mathbf{r}\,\mathrm{d}\mathbf{r}' \tag{9}$$

and the corresponding (static) screened Coulomb potential matrix elements at coupling strength λ

$$W_{pq,rs}^\lambda = \iint \phi_p(\mathbf{r})\phi_q(\mathbf{r})W^\lambda(\mathbf{r},\mathbf{r}')\phi_r(\mathbf{r}')\phi_s(\mathbf{r}')\mathrm{d}\mathbf{r}\,\mathrm{d}\mathbf{r}' \tag{10}$$

the BSE matrix elements, for singlet states, read

$$A_{ia,jb}^{\lambda,\mathrm{BSE}} = \delta_{ij}\delta_{ab}(\epsilon_a^{GW} - \epsilon_i^{GW}) + \lambda[2(ia|bj) - W_{ij,ab}^\lambda] \tag{11a}$$

$$B_{ia,jb}^{\lambda,\mathrm{BSE}} = \lambda[2(ia|jb) - W_{ib,aj}^\lambda] \tag{11b}$$

where ϵ_p^{GW} are the *GW* quasiparticle energies. In the standard BSE approach, W^λ is built within the direct RPA scheme, *i.e.*

$$W^\lambda(\mathbf{r},\mathbf{r}') = \int \frac{\epsilon_\lambda^{-1}(\mathbf{r},\mathbf{r}'';\omega = 0)}{|\mathbf{r}' - \mathbf{r}''|}\mathrm{d}\mathbf{r}'' \tag{12a}$$

$$\epsilon_\lambda(\mathbf{r},\mathbf{r}';\omega) = \delta(\mathbf{r} - \mathbf{r}') - \lambda\int \frac{\chi_0(\mathbf{r},\mathbf{r}'';\omega)}{|\mathbf{r}' - \mathbf{r}''|}\mathrm{d}\mathbf{r}'' \tag{12b}$$

with ϵ_λ the dielectric function at coupling constant λ and χ_0 the noninteracting polarizability. In the occupied-to-virtual orbital product basis, the spectral representation of W^λ can be written as follows in the case of real spatial orbitals

https://dx.doi.org/10.1021/acs.jpclett.0c00460
J. Phys. Chem. Lett. 2020, 11, 3536−3545

$$W^{\lambda}_{ij,ab}(\omega) = (ij|ab) + 2\sum_{m}^{OV} [ij|m]^{\lambda}[ab|m]^{\lambda} \times \left(\frac{1}{\omega - \Omega^{\lambda,\mathrm{RPA}}_{m} + i\eta} - \frac{1}{\omega + \Omega^{\lambda,\mathrm{RPA}}_{m} - i\eta} \right) \tag{13}$$

where the spectral weights at coupling strength λ read

$$[pq|m]^{\lambda} = \sum_{i}^{O}\sum_{a}^{V} (pq|ia)(\mathbf{X}^{\lambda}_{m} + \mathbf{Y}^{\lambda}_{m})_{ia} \tag{14}$$

In the case of complex orbitals, we refer the reader to ref 92 for a correct use of complex conjugation in the spectral representation of W. Note that, in the case of G_0W_0, the RPA neutral excitations in eq 13 are computed using the HF orbital energies.

In eq 13, η is a positive infinitesimal, and $\Omega^{\lambda,\mathrm{RPA}}_{m}$ are the direct (*i.e.*, without exchange) RPA neutral excitation energies computed by solving the linear eigenvalue problem (6) with the following matrix elements:

$$A^{\lambda,\mathrm{RPA}}_{ia,jb} = \delta_{ij}\delta_{ab}(\epsilon^{\mathrm{HF}}_{a} - \epsilon^{\mathrm{HF}}_{i}) + 2\lambda(ia|bj) \tag{15a}$$

$$B^{\lambda,\mathrm{RPA}}_{ia,jb} = 2\lambda(ia|jb) \tag{15b}$$

where $\epsilon^{\mathrm{HF}}_{p}$ are the Hartree−Fock (HF) orbital energies.

The relationship between the BSE formalism and the well-known RPAx (*i.e.*, RPA with exchange) approach can be obtained by switching off the screening so that W^{λ} reduces to the bare Coulomb potential v. In this limit, the GW quasiparticle energies reduce to the HF eigenvalues, and eqs 11a and 11b reduce to the RPAx equations:

$$A^{\lambda,\mathrm{RPAx}}_{ia,jb} = \delta_{ij}\delta_{ab}(\epsilon^{\mathrm{HF}}_{a} - \epsilon^{\mathrm{HF}}_{i}) + \lambda[2(ia|bj) - (ij|ab)] \tag{16a}$$

$$B^{\lambda,\mathrm{RPAx}}_{ia,jb} = \lambda[2(ia|jb) - (ib|aj)] \tag{16b}$$

The key quantity to define in the present context is the total BSE ground-state energy E^{BSE}. Although this choice is not unique,[67] we propose here to define it as

$$E^{\mathrm{BSE}} = E^{\mathrm{nuc}} + E^{\mathrm{HF}} + E^{\mathrm{BSE}}_{\mathrm{c}} \tag{17}$$

where E^{nuc} and E^{HF} are the nuclear repulsion energy and electronic ground-state HF energy (respectively), and

$$E^{\mathrm{BSE}}_{\mathrm{c}} = \frac{1}{2}\int_{0}^{1} \mathrm{Tr}(\mathbf{K}\mathbf{P}^{\lambda})\mathrm{d}\lambda \tag{18}$$

is the ground-state BSE correlation energy computed in the adiabatic connection framework, where

$$\mathbf{K} = \begin{pmatrix} \tilde{\mathbf{A}}^{\lambda=1} & \mathbf{B}^{\lambda=1} \\ \mathbf{B}^{\lambda=1} & \tilde{\mathbf{A}}^{\lambda=1} \end{pmatrix} \tag{19}$$

is the interaction kernel[67,76] [with $\tilde{A}^{\lambda}_{ia,jb} = 2\lambda(ia|jb)$];

$$\mathbf{P}^{\lambda} = \begin{pmatrix} \mathbf{Y}^{\lambda}(\mathbf{Y}^{\lambda})^{\mathrm{T}} & \mathbf{Y}^{\lambda}(\mathbf{X}^{\lambda})^{\mathrm{T}} \\ \mathbf{X}^{\lambda}(\mathbf{Y}^{\lambda})^{\mathrm{T}} & \mathbf{X}^{\lambda}(\mathbf{X}^{\lambda})^{\mathrm{T}} \end{pmatrix} - \begin{pmatrix} \mathbf{0} & \mathbf{0} \\ \mathbf{0} & \mathbf{1} \end{pmatrix} \tag{20}$$

is the correlation part of the two-electron density matrix at interaction strength λ, and Tr denotes the matrix trace. Note that the present definition of the BSE correlation energy (see eq 18), which we refer to as BSE@GW@HF in the following, has been named "XBS" for "extended Bethe−Salpeter" by Holzer et al.[67] For the sake of completeness, comparisons between the extended and regular BSE schemes can be found in the Supporting Information. In contrast to DFT where the electron density is fixed along the adiabatic path, in the present formalism, the density is not maintained as λ varies. Therefore, an additional contribution to eq 18 originating from the variation of the Green's function along the adiabatic connection should be, in principle, added. However, as commonly done within RPA and RPAx,[67,74,75,93] we shall neglect it in the present study.

Equation 18 can also be straightforwardly applied to RPA and RPAx, the only difference being the expressions of $\mathbf{A}^{\lambda}$ and $\mathbf{B}^{\lambda}$ used to obtain the eigenvectors $\mathbf{X}^{\lambda}$ and $\mathbf{Y}^{\lambda}$ entering in the definition of $\mathbf{P}^{\lambda}$ (see eq 20). For RPA, these expressions have been provided in eqs 15a and 15b, and their RPAx analogues are in eqs 16a and 16b. In the following, we will refer to these two types of calculations as RPA@HF and RPAx@HF, respectively. Finally, we will also consider the RPA@GW@HF scheme which consists of replacing the HF orbital energies in eq 15a by the GW quasiparticles energies.

Note that, for spin-restricted closed-shell molecular systems around their equilibrium geometry (such as the ones studied here), one rarely encounters singlet instabilities as these systems can be classified as weakly correlated. However, singlet instabilities may appear in the presence of strong correlation, *e.g.*, when the bonds are stretched, hampering in particular the calculation of atomization energies.[67] Even for weakly correlated systems, triplet instabilities are much more common, but triplet excitations do not contribute to the correlation energy in the ACFDT formulation.[74−76]

The restricted HF formalism has been systematically employed in the present study. All the GW calculations performed to obtain the screened Coulomb operator and the quasiparticle energies are done using a (restricted) HF starting point, which is an adequate choice in the case of the (small) systems that we have considered here. Perturbative GW (or G_0W_0)[37,94] calculations are employed as starting points to compute the BSE neutral excitations. In the case of G_0W_0, the quasiparticle energies are obtained by linearizing the frequency-dependent quasiparticle equation. Further details about our implementation of G_0W_0 can be found in refs 80 and 81. Finally, the infinitesimal η is set to zero for all calculations. The numerical integration required to compute the correlation energy along the adiabatic path (see eq 18) is performed with a 21-point Gauss−Legendre quadrature. Comparison with the so-called plasmon (or trace) formula[73] at the RPA level has confirmed the excellent accuracy of this quadrature scheme over λ.

For comparison purposes, we have also computed the PES at the second-order Møller−Plesset perturbation theory (MP2), as well as with various increasingly accurate CC methods, namely, CC2,[95] CCSD,[96] and CC3.[97] These calculations have been performed with DALTON[98] and PSI4.[99] The computational cost of these methods, in their usual implementation, scale as $O(N^5)$, $O(N^5)$, $O(N^6)$, and $O(N^7)$, respectively. As shown in refs 100 and 101, CC3 provides extremely accurate ground-state (and excited-state) geometries and will be taken as the reference in the present study. In order to check further the overall accuracy of CC3, we have performed CCSDT and CCSDT(Q) calculations[102] at equilibrium bond lengths. These results are provided in the Supporting Information and clearly evidence the excellent accuracy of CC3, the maximum absolute

https://dx.doi.org/10.1021/acs.jpclett.0c00460
J. Phys. Chem. Lett. 2020, 11, 3536−3545

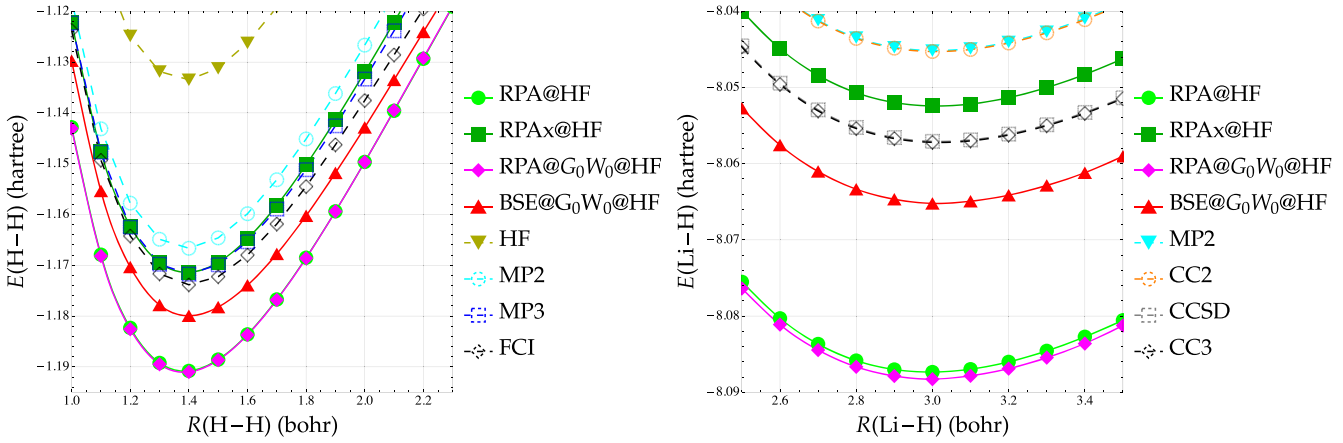

Figure 1. Ground-state PES of H_2 (left) and LiH (right) around their respective equilibrium geometry obtained at various levels of theory with the cc-pVQZ basis set.

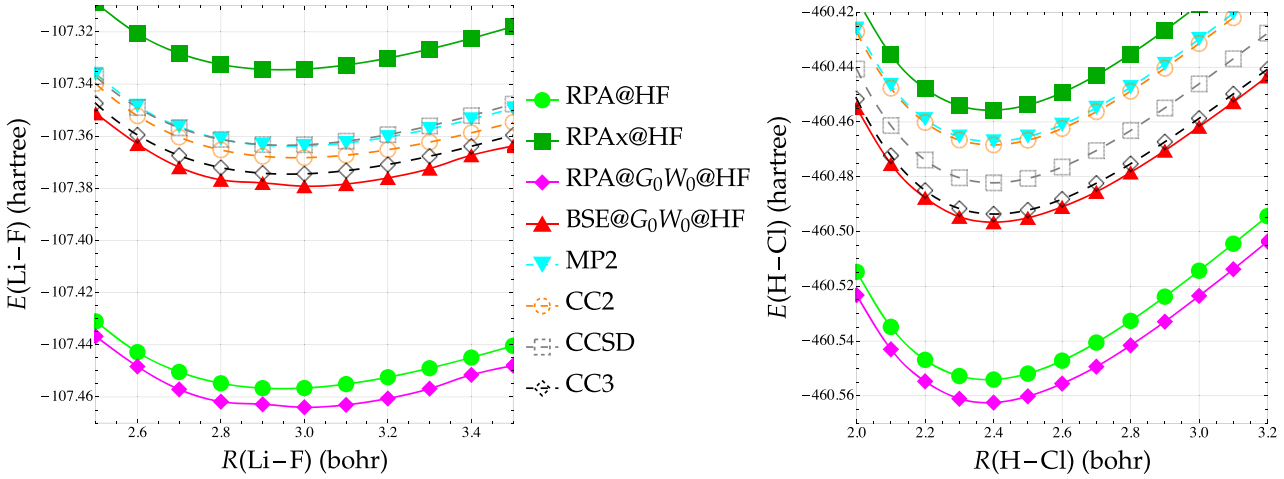

Figure 2. Ground-state PES of LiF (left) and HCl (right) around their respective equilibrium geometry obtained at various levels of theory with the cc-pVQZ basis set.

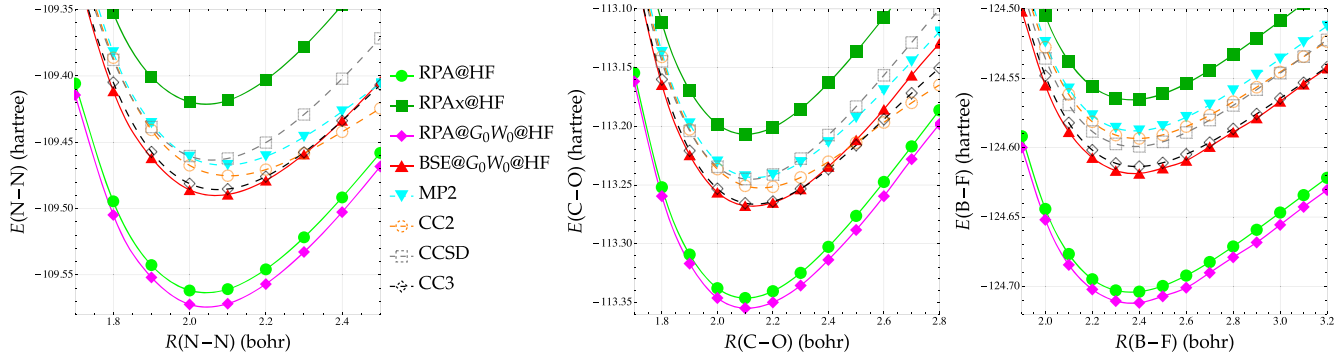

Figure 3. Ground-state PES of the isoelectronic series N_2 (left), CO (center), and BF (right) around their respective equilibrium geometry obtained at various levels of theory with the cc-pVQZ basis set.

deviation between CC3 and CCSDT(Q) being 0.2% at equilibrium. All the other calculations have been performed with our locally developed *GW* software.[80,81] As one-electron basis sets, we employ the Dunning family (cc-pVXZ) defined with Cartesian Gaussian functions. Unless otherwise stated, the frozen-core approximation is not applied in order to provide a fair comparison between methods. We have, however, found that our conclusions hold within the frozen-core approximation (see the Supporting Information).

Because eq 18 requires the entire BSE singlet excitation spectrum for each quadrature point, we perform several complete diagonalizations of the $OV \times OV$ BSE linear response matrix (see eq 7), which corresponds to an $O(O^3V^3) = O(N^6)$ computational cost. This step is, by far, the computational bottleneck in our current implementation. However, we are currently pursuing different avenues to lower the formal scaling and practical cost of this step by computing the two-electron

https://dx.doi.org/10.1021/acs.jpclett.0c00460
J. Phys. Chem. Lett. 2020, 11, 3536−3545

density matrix of eq 20 via a quadrature in frequency space.[82,103]

In order to illustrate the performance of the BSE-based adiabatic connection formulation, we compute the ground-state PES of several closed-shell diatomic molecules around their equilibrium geometry: H_2, LiH, LiF, HCl, N_2, CO, BF, and F_2. The PESs of these molecules are represented in Figures 1, 2, 3, and 4, while the computed equilibrium distances and

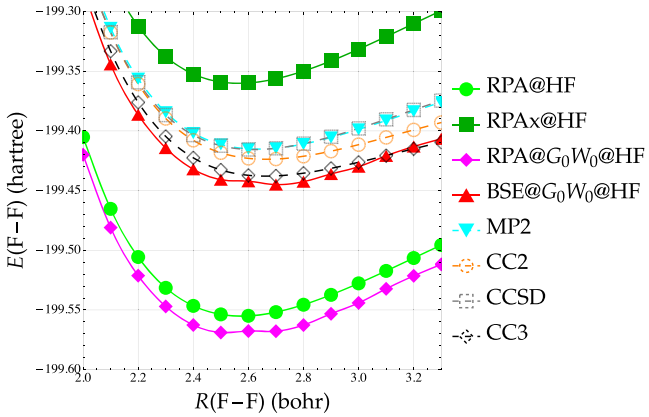

Figure 4. Ground-state PES of F_2 around its equilibrium geometry obtained at various levels of theory with the cc-pVQZ basis set.

correlation energies are gathered in Table 1. Both of these properties are computed with Dunning's cc-pVQZ basis set. Graphs and tables for the corresponding double- and triple-ζ basis sets (as well as harmonic frequencies) can be found in the Supporting Information.

Let us start with the two smallest molecules, H_2 and LiH. Their PESs computed with the cc-pVQZ basis are reported in Figure 1. For H_2, we take as reference the full configuration interaction (FCI) energies,[104] and we also report the MP2 curve and its third-order variant (MP3), which improves upon MP2 toward FCI. RPA@HF and RPA@G_0W_0@HF yield almost identical results, and both significantly overestimate the FCI correlation energy, while RPAx@HF and BSE@G_0W_0@HF slightly over- and undershoot the FCI energy, respectively, RPAx@HF yielding the best match to FCI in the case of H_2. Interestingly, the BSE@G_0W_0@HF scheme yields a more accurate equilibrium bond length than any other method irrespective of the basis set (see Table I in the Supporting Information). For example, BSE@G_0W_0@HF/cc-pVQZ is off by only 0.003 bohr as compared to FCI/cc-pVQZ, while RPAx@HF, MP2, and CC2 underestimate the bond length by 0.008, 0.011, and 0.011 bohr, respectively. The RPA-based schemes are much less accurate, with even shorter equilibrium bond lengths. This is a general trend that is magnified in larger systems as the ones discussed below.

Despite the shallow nature of its PES, the scenario is almost identical for LiH for which we report the CC2, CCSD, and CC3 energies in addition to MP2 energies. In this case, RPAx@HF and BSE@G_0W_0@HF nestle the CCSD and CC3 energy curves, these surfaces running almost perfectly parallel to one another. Here again, the BSE@G_0W_0@HF/cc-pVQZ equilibrium bond length is extremely accurate (3.017 bohr) as compared to CC3/cc-pVQZ (3.019 bohr).

The cases of LiF and HCl (see Figure 2) are chemically interesting as they correspond to strongly polarized bonds toward the halogen atoms which are much more electro-negative than the first-column elements. For these partially ionic bonds, the performance of BSE@G_0W_0@HF is terrific with an almost perfect match to the CC3 curve. Maybe surprisingly, BSE@G_0W_0@HF is on par with both CC2 and CCSD and outperforms RPAx@HF by a big margin, the latter fact being also observed for the other diatomics discussed below. Interestingly, while CCSD and CC2 systematically underestimate the total energy, the BSE@G_0W_0@HF energy is always lower than the reference CC3 energy. This observation not only is true for LiF and HCl but also holds for every single system that is considered herein. Moreover, this is consistent with the study by Maggio and Kresse on the HEG showing that BSE slightly overestimates the correlation energy as compared to QMC reference data.[72] Similarly, the much larger overestimation of the correlation energy that we observe at the RPA@*GW* level was also observed for the HEG. Care must be taken however in drawing comparisons because the HEG study of ref 72 was performed starting with LDA eigenstates.

For HCl, the data reported in Table 1 show that the BSE@G_0W_0@HF equilibrium bond length is again in very good agreement with its CC3 counterpart as it underestimates the bond lengths by only a few hundredths of a bohr. However, in the case of LiF, the attentive reader can observe a small "glitch" in the *GW*-based curves very close to their minimum. As observed in refs 78−80 and explained in detail in refs 81 and 82, these irregularities, which make particularly tricky the location of the minima, are due to "jumps" between distinct solutions of the *GW* quasiparticle equation. Including a broadening via an increase of the η value entering in the expression of the *GW* self-energy and the screened Coulomb operator softens the problem but does not remove it completely. When irregularities are present in the PES, we have fitted a Morse potential of the form $M(R) = D_0\{1 - \exp[-\alpha(R - R_{eq})]\}^2$ to the PES in order to provide an estimate of the equilibrium bond length.[105] These values are reported in parentheses in Table 1. For the smooth PES where one can obtain both the genuine minimum and the fitted minimum (*i.e.*, based on the Morse curve), this procedure has been shown to be very accurate with an error of the order of 10^{-3} bohr in most cases. We note that these irregularities are much smaller than the differences between the BSE and the other RPA-like techniques (RPA, RPAx, and RPA@*GW*), leaving BSE unambiguously more accurate than these approaches.

Let us now look at the isoelectronic series N_2, CO, and BF, which have a decreasing bond order (from triple to single bond). The conclusions drawn for the previous systems also apply to these molecules. In particular, as shown in Figure 3, the performance of BSE@G_0W_0@HF is outstanding with an error of the order of 1% on the correlation energy. Importantly, it systematically outperforms both CC2 and CCSD. One can notice some irregularities in the PES of BF with the cc-pVDZ et cc-pVTZ basis sets (see the Supporting Information). The PESs of N_2 and CO are smooth though and yield accurate equilibrium bond lengths once more. Indeed, at the BSE@G_0W_0@HF/cc-pVQZ level of theory, we obtain 2.065, 2.134, and 2.385 bohr for N_2, CO, and BF, respectively, which have to be compared with the CC3/cc-pVQZ values of 2.075, 2.136, and 2.390 bohr, respectively.

As a final example, we consider the F_2 molecule, a notoriously difficult case to treat because of the weakness of its covalent bond (see Figure 4) and hence its relatively long equilibrium bond length (2.663 bohr at the CC3/cc-pVQZ

https://dx.doi.org/10.1021/acs.jpclett.0c00460
J. Phys. Chem. Lett. 2020, 11, 3536−3545

Table 1. Equilibrium Bond Length (R_{eq}, bohr) and Correlation Energy (E_c, millihartree) for the Ground State of Diatomic Molecules Obtained with the cc-pVQZ Basis Set at Various Levels of Theory[a]

	equilibrium bond length, R_{eq} (bohr)							
method	H_2[b]	LiH	LiF	HCl	N_2	CO	BF	F_2
CC3	1.402	3.019	2.963	2.403	2.075	2.136	2.390	2.663
CCSD	1.402[+0.0%]	3.020[+0.0%]	2.953[−0.3%]	2.398[−0.2%]	2.059[−0.8%]	2.118[−0.8%]	2.380[−0.4%]	2.621[−1.6%]
CC2	1.391[−0.8%]	3.010[−0.3%]	2.982[+0.6%]	2.396[−0.3%]	2.106[+1.5%]	2.156[+0.9%]	2.393[+0.1%]	2.665[+0.1%]
MP2	1.391[−0.8%]	3.008[−0.4%]	2.970[+0.2%]	2.395[−0.3%]	2.091[+0.8%]	2.137[+0.1%]	2.382[−0.3%]	2.634[−1.1%]
BSE@G_0W_0@HF	1.399[−0.2%]	3.017[−0.1%]	(2.973)[+0.3%]	2.400[−0.1%]	2.065[−0.5%]	2.134[−0.1%]	2.385[−0.2%]	(2.638)[−0.9%]
RPA@G_0W_0@HF	1.382[−1.4%]	2.997[−0.7%]	(2.965)[+0.1%]	2.370[−1.5%]	2.043[−1.5%]	2.132[−0.2%]	2.365[−1.1%]	(2.571)[−3.5%]
RPAx@HF	1.394[−0.6%]	3.011[−0.3%]	2.944[−0.6%]	2.391[−0.5%]	2.041[−1.6%]	2.104[−1.5%]	2.366[−1.0%]	2.565[−3.7%]
RPA@HF	1.386[−1.1%]	2.994[−0.8%]	2.946[−0.6%]	2.382[−0.9%]	2.042[−1.6%]	2.103[−1.5%]	2.364[−1.1%]	2.573[−3.4%]
	Correlation energy, E_c (millihartree)							
method	H_2[b]	LiH	LiF	HCl	N_2	CO	BF	F_2
CC3	40.4	70.0	383.7	382.2	494.4	477.6	447.5	668.9
CCSD	40.4[+0.0%]	69.8[−0.2%]	372.6[−2.9%]	370.8[−3.0%]	470.6[−4.8%]	455.2[−4.7%]	432.9[−3.3%]	644.0[−3.7%]
CC2	33.3[−17.6%]	57.2[−18.1%]	376.7[−1.8%]	356.9[−6.6%]	488.0[−1.3%]	465.5[−2.5%]	427.3[−4.5%]	654.9[−2.1%]
MP2	33.2[−17.9%]	57.9[−17.2%]	373.0[−2.8%]	355.7[−6.9%]	478.0[−3.3%]	455.0[−4.7%]	421.6[−5.8%]	644.3[−3.7%]
BSE@G_0W_0@HF	46.5[+15.1%]	78.0[+11.4%]	388.3[+1.2%]	385.1[+0.8%]	497.9[+0.7%]	480.0[+0.5%]	452.3[+1.1%]	673.9[+0.8%]
RPA@G_0W_0@HF	57.6[+42.6%]	101.1[+44.5%]	473.1[+23.3%]	451.2[+18.1%]	580.3[+17.4%]	566.5[+18.6%]	545.5[+21.9%]	794.3[+18.8%]
RPAx@HF	37.9[−6.2%]	65.2[−6.8%]	343.6[−10.5%]	344.2[−9.9%]	427.2[−13.6%]	416.3[−12.8%]	399.1[−10.8%]	586.1[−12.4%]
RPA@HF	57.3[+42.0%]	100.2[+43.2%]	465.9[+21.4%]	442.7[+15.8%]	569.4[+15.2%]	555.9[+16.4%]	537.7[+20.2%]	781.3[+16.8%]

[a]For each system and each method, the correlation energy is computed at its respective equilibrium bond length (*i.e.*, $R = R_{eq}$). When irregularities appear in the PES, the R_{eq} values are reported in parentheses and they have been obtained by fitting a Morse potential to the PES. The error (in %) compared to the reference CC3 values are reported in square brackets. [b]For H_2, both CC3 and CCSD are equivalent to FCI.

https://dx.doi.org/10.1021/acs.jpclett.0c00460
J. Phys. Chem. Lett. 2020, 11, 3536−3545

level). Similarly to what is observed for LiF and BF, there are irregularities near the minimum of the G_0W_0-based curves. However, BSE@G_0W_0@HF is the closest to the CC3 curve, with an error on the correlation energy of 1% and an estimated bond length of 2.640 bohr (via a Morse fit) at the BSE@G_0W_0@HF/cc-pVQZ level. Note that, for this system, triplet (and then singlet) instabilities appear for quite short bond lengths. However, around the equilibrium structure, we have not encountered any instabilities. This is an important outcome of the present study as the difficulties encountered at large interatomic distances (*i.e.*, close to the dissociation limit) do not prevent the BSE approach from being potentially useful and accurate in the vicinity of equilibrium distances. Furthermore, preliminary calculations could not detect any singlet instabilities in the vicinity of the lowest singlet excited-state minimum.

As a final remark, we mention that although we have considered here only a limited set of compounds, our correlation energy mean absolute error (MAE) with BSE@G_0W_0@HF of 4.7 mHa (as compared to CC3) is significantly less than the one obtained with MP2, CC2, and CCSD (18.2, 13.1, and 13.5 mHa, respectively). For comparison, the RPA-related formalisms return larger MAEs of 75.6, 43.1, and 68.2 mHa for BSE@G_0W_0@HF, RPAx@HF, and RPA@HF, respectively.

In this Letter, we hope to have illustrated that the ACFDT@BSE formalism is a promising methodology for the computation of accurate ground-state PESs and their corresponding equilibrium structures. To do so, we have shown that calculating the BSE correlation energy computed within the ACFDT framework yields extremely accurate PESs around equilibrium. Their accuracy near the dissociation limit remains an open question.[66,67,93,106,107] We have illustrated this for eight diatomic molecules for which we have also computed reference ground-state energies using coupled cluster methods (CC2, CCSD, and CC3). Moreover, because triplet states do not contribute to the ACFDT correlation energy and singlet instabilities do not appear for weakly correlated systems around their equilibrium structure, the present scheme does not suffer from singlet or triplet instabilities. However, we have also observed, in some cases, unphysical irregularities on the ground-state PES due to the appearance of discontinuities as a function of the bond length for some of the *GW* quasiparticle energies. Such an unphysical behavior stems from defining the quasiparticle energy as the solution of the quasiparticle equation with the largest spectral weight in cases where several solutions can be found. This shortcoming has been thoroughly described in several previous studies.[78−82] We believe that this central issue must be resolved if one wants to expand the applicability of the present method.

■ ASSOCIATED CONTENT

Supporting Information

The Supporting Information is available free of charge at https://pubs.acs.org/doi/10.1021/acs.jpclett.0c00460.

Additional potential energy curves computed with other basis sets and within the frozen-core approximation, tables gathering harmonic frequencies, equilibrium distances for smaller basis sets (cc-pVDZ and cc-pVTZ), CC3, CCSDT, and CCSDT(Q) total energies, as well as comparisons between the extended and regular BSE schemes (correlation energies at equilibrium geometries) (PDF)

■ AUTHOR INFORMATION

Corresponding Authors

Pierre-François Loos − *Laboratoire de Chimie et Physique Quantiques (UMR 5626), Université de Toulouse, CNRS, UPS, 31077 Toulouse, France;* orcid.org/0000-0003-0598-7425; Email: loos@irsamc.ups-tlse.fr

Denis Jacquemin − *Laboratoire CEISAM - UMR CNRS 6230, Université de Nantes, 44322 Nantes, France;* orcid.org/0000-0002-4217-0708; Email: denis.jacquemin@univ-nantes.fr

Xavier Blase − *Université Grenoble Alpes, CNRS, Institut NEEL, F-38042 Grenoble, France;* orcid.org/0000-0002-0201-9093; Email: xavier.blase@neel.cnrs.fr

Authors

Anthony Scemama − *Laboratoire de Chimie et Physique Quantiques (UMR 5626), Université de Toulouse, CNRS, UPS, 31077 Toulouse, France*

Ivan Duchemin − *Université Grenoble Alpes, CEA, IRIG-MEM-L Sim, 38054 Grenoble, France;* orcid.org/0000-0003-4713-1174

Complete contact information is available at: https://pubs.acs.org/10.1021/acs.jpclett.0c00460

Notes

The authors declare no competing financial interest.

■ ACKNOWLEDGMENTS

P.-F.L. thanks Julien Toulouse for enlightening discussions about RPA, and X.B. is indebted to Valerio Olevano for numerous discussions. This work was performed using HPC resources from GENCI-TGCC (Grant No. 2019-A0060801738), CALMIP (Toulouse) under allocation 2020-18005, and the CCIPL center installed in Nantes. Funding from the "*Centre National de la Recherche Scientifique*" is acknowledged. This work has also been supported through the EUR Grant NanoX ANR-17-EURE-0009 in the framework of the "*Programme des Investissements d'Avenir*".

■ REFERENCES

(1) Runge, E.; Gross, E. K. U. Density-Functional Theory for Time-Dependent Systems. *Phys. Rev. Lett.* **1984**, *52*, 997−1000.
(2) Casida, M. E. In *Time-Dependent Density Functional Response Theory for Molecules*; Chong, D. P., Ed.; Recent Advances in Density Functional Methods; World Scientific, Singapore, 1995; pp 155−192.
(3) Salpeter, E. E.; Bethe, H. A. A Relativistic Equation for Bound-State Problems. *Phys. Rev.* **1951**, *84*, 1232.
(4) Strinati, G. Application of the Green's Functions Method to the Study of the Optical Properties of Semiconductors. *Riv. Nuovo Cimento* **1988**, *11*, 1−86.
(5) Albrecht, S.; Reining, L.; Del Sole, R.; Onida, G. Ab Initio Calculation of Excitonic Effects in the Optical Spectra of Semiconductors. *Phys. Rev. Lett.* **1998**, *80*, 4510−4513.
(6) Rohlfing, M.; Louie, S. G. Electron-Hole Excitations in Semiconductors and Insulators. *Phys. Rev. Lett.* **1998**, *81*, 2312−2315.
(7) Benedict, L. X.; Shirley, E. L.; Bohn, R. B. Optical Absorption of Insulators and the Electron-Hole Interaction: An Ab Initio Calculation. *Phys. Rev. Lett.* **1998**, *80*, 4514−4517.
(8) van der Horst, J.-W.; Bobbert, P. A.; Michels, M. A. J.; Brocks, G.; Kelly, P. J. Ab Initio Calculation of the Electronic and Optical

Excitations in Polythiophene: Effects of Intra- and Interchain Screening. *Phys. Rev. Lett.* **1999**, *83*, 4413−4416.
(9) Ma, Y.; Rohlfing, M.; Molteni, C. Excited States of Biological Chromophores Studied Using Many-Body Perturbation Theory: Effects of Resonant-Antiresonant Coupling and Dynamical Screening. *Phys. Rev. B: Condens. Matter Mater. Phys.* **2009**, *80*, 241405.
(10) Puschnig, P.; Ambrosch-Draxl, C. Suppression of Electron-Hole Correlations in 3D Polymer Materials. *Phys. Rev. Lett.* **2002**, *89*, No. 056405.
(11) Tiago, M. L.; Northrup, J. E.; Louie, S. G. Ab Initio Calculation of the Electronic and Optical Properties of Solid Pentacene. *Phys. Rev. B: Condens. Matter Mater. Phys.* **2003**, *67*, 115212.
(12) Palummo, M.; Hogan, C.; Sottile, F.; Bagalá, P.; Rubio, A. Ab Initio Electronic and Optical Spectra of Free-Base Porphyrins: The Role of Electronic Correlation. *J. Chem. Phys.* **2009**, *131*, No. 084102.
(13) Rocca, D.; Lu, D.; Galli, G. Ab Initio Calculations of Optical Absorption Spectra: Solution of the Bethe−Salpeter Equation Within Density Matrix Perturbation Theory. *J. Chem. Phys.* **2010**, *133*, 164109.
(14) Sharifzadeh, S.; Biller, A.; Kronik, L.; Neaton, J. B. Quasiparticle and Optical Spectroscopy of the Organic Semiconductors Pentacene and PTCDA From First Principles. *Phys. Rev. B: Condens. Matter Mater. Phys.* **2012**, *85*, 125307.
(15) Cudazzo, P.; Gatti, M.; Rubio, A. Excitons in Molecular Crystals From First-Principles Many-Body Perturbation Theory: Picene Versus Pentacene. *Phys. Rev. B: Condens. Matter Mater. Phys.* **2012**, *86*, 195307.
(16) Boulanger, P.; Jacquemin, D.; Duchemin, I.; Blase, X. Fast and Accurate Electronic Excitations in Cyanines with the Many-Body Bethe−Salpeter Approach. *J. Chem. Theory Comput.* **2014**, *10*, 1212−1218.
(17) Ljungberg, M. P.; Koval, P.; Ferrari, F.; Foerster, D.; Sánchez-Portal, D. Cubic-Scaling Iterative Solution of the Bethe-Salpeter Equation for Finite Systems. *Phys. Rev. B: Condens. Matter Mater. Phys.* **2015**, *92*, No. 075422.
(18) Hirose, D.; Noguchi, Y.; Sugino, O. All-Electron GW+Bethe-Salpeter Calculations on Small Molecules. *Phys. Rev. B: Condens. Matter Mater. Phys.* **2015**, *91*, 205111.
(19) Cocchi, C.; Draxl, C. Bound Excitons and Many-Body Effects in X-Ray Absorption Spectra of Azobenzene-Functionalized Self-Assembled Monolayers. *Phys. Rev. B: Condens. Matter Mater. Phys.* **2015**, *92*, 205105.
(20) Ziaei, V.; Bredow, T. Simple many-body based screening mixing ansatz for improvement of *GW*/Bethe-Salpeter equation excitation energies of molecular systems. *Phys. Rev. B: Condens. Matter Mater. Phys.* **2017**, *96*, 195115.
(21) Refaely-Abramson, S.; da Jornada, F. H.; Louie, S. G.; Neaton, J. B. Origins of Singlet Fission in Solid Pentacene from an ab initio Green's Function Approach. *Phys. Rev. Lett.* **2017**, *119*, 267401.
(22) González, L.; Escudero, D.; Serrano-Andrès, L. Progress and Challenges in the Calculation of Electronic Excited States. *ChemPhysChem* **2012**, *13*, 28−51.
(23) Loos, P. F.; Scemama, A.; Jacquemin, D. The Quest for Highly-Accurate Excitation Energies: a Computational Perspective. *J. Phys. Chem. Lett.* **2020**, *11*, 2374.
(24) Jacquemin, D.; Duchemin, I.; Blase, X. Benchmarking the Bethe−Salpeter Formalism on a Standard Organic Molecular Set. *J. Chem. Theory Comput.* **2015**, *11*, 3290−3304.
(25) Bruneval, F.; Hamed, S. M.; Neaton, J. B. A Systematic Benchmark of the *Ab Initio* Bethe-Salpeter Equation Approach for Low-Lying Optical Excitations of Small Organic Molecules. *J. Chem. Phys.* **2015**, *142*, 244101.
(26) Hung, L.; da Jornada, F. H.; Souto-Casares, J.; Chelikowsky, J. R.; Louie, S. G.; Ogut, S. Excitation Spectra of Aromatic Molecules within a Real-Space GW-BSE Formalism: Role of Self-Consistency and Vertex Corrections. *Phys. Rev. B: Condens. Matter Mater. Phys.* **2016**, *94*, No. 085125.
(27) Hung, L.; Bruneval, F.; Baishya, K.; Öğüt, S. Benchmarking the *GW* Approximation and Bethe−Salpeter Equation for Groups IB and IIB Atoms and Monoxides. *J. Chem. Theory Comput.* **2017**, *13*, 2135−2146.
(28) Krause, K.; Klopper, W. Implementation of the Bethe-Salpeter Equation in the Turbomole Program. *J. Comput. Chem.* **2017**, *38*, 383−388.
(29) Jacquemin, D.; Duchemin, I.; Blondel, A.; Blase, X. Benchmark of Bethe-Salpeter for Triplet Excited-States. *J. Chem. Theory Comput.* **2017**, *13*, 767−783.
(30) Blase, X.; Duchemin, I.; Jacquemin, D. The Bethe−Salpeter Equation in Chemistry: Relations with TD-DFT, Applications and Challenges. *Chem. Soc. Rev.* **2018**, *47*, 1022−1043.
(31) Garcia-Lastra, J. M.; Thygesen, K. S. Renormalization of Optical Excitations in Molecules Near a Metal Surface. *Phys. Rev. Lett.* **2011**, *106*, 187402.
(32) Blase, X.; Attaccalite, C. Charge-Transfer Excitations in Molecular Donor-Acceptor Complexes Within the Many-Body Bethe-Salpeter Approach. *Appl. Phys. Lett.* **2011**, *99*, 171909.
(33) Baumeier, B.; Andrienko, D.; Rohlfing, M. Frenkel and Charge-Transfer Excitations in Donor−Acceptor Complexes From Many-Body Green's Functions Theory. *J. Chem. Theory Comput.* **2012**, *8*, 2790−2795.
(34) Duchemin, I.; Deutsch, T.; Blase, X. Short-Range to Long-Range Charge-Transfer Excitations in the Zincbacteriochlorin-Bacteriochlorin Complex: A Bethe-Salpeter Study. *Phys. Rev. Lett.* **2012**, *109*, 167801.
(35) Cudazzo, P.; Gatti, M.; Rubio, A.; Sottile, F. Frenkel Versus Charge-Transfer Exciton Dispersion in Molecular Crystals. *Phys. Rev. B: Condens. Matter Mater. Phys.* **2013**, *88*, 195152.
(36) Ziaei, V.; Bredow, T. GW-BSE Approach on S1 Vertical Transition Energy of Large Charge Transfer Compounds: A Performance Assessment. *J. Chem. Phys.* **2016**, *145*, 174305.
(37) Hybertsen, M. S.; Louie, S. G. Electron Correlation in Semiconductors and Insulators: Band Gaps and Quasiparticle Energies. *Phys. Rev. B: Condens. Matter Mater. Phys.* **1986**, *34*, 5390−5413.
(38) Shishkin, M.; Kresse, G. Self-Consistent G W Calculations for Semiconductors and Insulators. *Phys. Rev. B: Condens. Matter Mater. Phys.* **2007**, *75*, 235102.
(39) Blase, X.; Attaccalite, C.; Olevano, V. First-Principles GW Calculations for Fullerenes, Porphyrins, Phtalocyanine, and Other Molecules of Interest for Organic Photovoltaic Applications. *Phys. Rev. B: Condens. Matter Mater. Phys.* **2011**, *83*, 115103.
(40) Faber, C.; Attaccalite, C.; Olevano, V.; Runge, E.; Blase, X. First-Principles GW Calculations for DNA and RNA Nucleobases. *Phys. Rev. B: Condens. Matter Mater. Phys.* **2011**, *83*, 115123.
(41) Rangel, T.; Hamed, S. M.; Bruneval, F.; Neaton, J. B. Evaluating the GW Approximation with CCSD(T) for Charged Excitations Across the Oligoacenes. *J. Chem. Theory Comput.* **2016**, *12*, 2834−2842.
(42) Kaplan, F.; Harding, M. E.; Seiler, C.; Weigend, F.; Evers, F.; van Setten, M. J. Quasi-Particle Self-Consistent *GW* for Molecules. *J. Chem. Theory Comput.* **2016**, *12*, 2528−2541.
(43) Gui, X.; Holzer, C.; Klopper, W. Accuracy Assessment of *GW* Starting Points for Calculating Molecular Excitation Energies Using the Bethe−Salpeter Formalism. *J. Chem. Theory Comput.* **2018**, *14*, 2127−2136.
(44) Levine, B. G.; Ko, C.; Quenneville, J.; MartÍnez, T. J. Conical Intersections and Double Excitations in Time-Dependent Density Functional Theory. *Mol. Phys.* **2006**, *104*, 1039−1051.
(45) Tozer, D. J.; Handy, N. C. On the Determination of Excitation Energies Using Density Functional Theory. *Phys. Chem. Chem. Phys.* **2000**, *2*, 2117−2121.
(46) Huix-Rotllant, M.; Natarajan, B.; Ipatov, A.; Muhavini Wawire, C.; Deutsch, T.; Casida, M. E. Assessment of Noncollinear Spin-Flip Tamm−Dancoff Approximation Time-Dependent Density-Functional Theory for the Photochemical Ring-Opening of Oxirane. *Phys. Chem. Chem. Phys.* **2010**, *12*, 12811.
(47) Elliott, P.; Goldson, S.; Canahui, C.; Maitra, N. T. Perspectives on Double-Excitations in TDDFT. *Chem. Phys.* **2011**, *391*, 110−119.

https://dx.doi.org/10.1021/acs.jpclett.0c00460
J. Phys. Chem. Lett. 2020, 11, 3536−3545

(48) Romaniello, P.; Sangalli, D.; Berger, J. A.; Sottile, F.; Molinari, L. G.; Reining, L.; Onida, G. Double Excitations in Finite Systems. *J. Chem. Phys.* **2009**, *130*, No. 044108.
(49) Sangalli, D.; Romaniello, P.; Onida, G.; Marini, A. Double Excitations in Correlated Systems: A Many−Body Approach. *J. Chem. Phys.* **2011**, *134*, No. 034115.
(50) Loos, P.-F.; Boggio-Pasqua, M.; Scemama, A.; Caffarel, M.; Jacquemin, D. Reference Energies for Double Excitations. *J. Chem. Theory Comput.* **2019**, *15*, 1939−1956.
(51) Furche, F.; Ahlrichs, R. Adiabatic Time-Dependent Density Functional Methods for Excited State Properties. *J. Chem. Phys.* **2002**, *117*, 7433.
(52) Bernardi, F.; Olivucci, M.; Robb, M. A. Potential Energy Surface Crossings in Organic Photochemistry. *Chem. Soc. Rev.* **1996**, *25*, 321.
(53) Olivucci, M. *Computational Photochemistry*; Elsevier Science: Amsterdam, 2010; OCLC: 800555856..
(54) Navizet, I.; Liu, Y.-J.; Ferre, N.; Roca-Sanjuan, D.; Lindh, R. The Chemistry of Bioluminescence: An Analysis of Chemical Functionalities. *ChemPhysChem* **2011**, *12*, 3064−3076.
(55) Robb, M. A.; Garavelli, M.; Olivucci, M.; Bernardi, F.In *Reviews in Computational Chemistry*; Lipkowitz, K. B., Boyd, D. B., Eds.; John Wiley & Sons, Inc.: Hoboken, NJ, 2007; pp 87−146.
(56) Lazzeri, M.; Attaccalite, C.; Wirtz, L.; Mauri, F. Impact of the Electron-Electron Correlation on Phonon Dispersion: Failure of LDA and GGA DFT Functionals in Graphene and Graphite. *Phys. Rev. B: Condens. Matter Mater. Phys.* **2008**, *78*, No. 081406.
(57) Faber, C.; Janssen, J. L.; Côté, M.; Runge, E.; Blase, X. Electron-phonon coupling in the C_{60} fullerene within the many-body *GW* approach. *Phys. Rev. B: Condens. Matter Mater. Phys.* **2011**, *84*, 155104.
(58) Yin, Z. P.; Kutepov, A.; Kotliar, G. Correlation-Enhanced Electron-Phonon Coupling: Applications of *GW* and Screened Hybrid Functional to Bismuthates, Chloronitrides, and Other High-T_c Superconductors. *Phys. Rev. X* **2013**, *3*, No. 021011.
(59) Faber, C.; Boulanger, P.; Attaccalite, C.; Cannuccia, E.; Duchemin, I.; Deutsch, T.; Blase, X. Exploring Approximations to the *GW* Self-Energy Ionic Gradients. *Phys. Rev. B: Condens. Matter Mater. Phys.* **2015**, *91*, 155109.
(60) Monserrat, B. Correlation Effects on Electron-Phonon Coupling in Semiconductors: Many-Body Theory Along Thermal Lines. *Phys. Rev. B: Condens. Matter Mater. Phys.* **2016**, *93*, 100301.
(61) Li, Z.; Antonius, G.; Wu, M.; da Jornada, F. H.; Louie, S. G. Electron-Phonon Coupling from Ab Initio Linear-Response Theory within the *GW* Method: Correlation-Enhanced Interactions and Superconductivity in $Ba_{1-x}K_xBiO_3$. *Phys. Rev. Lett.* **2019**, *122*, 186402.
(62) Ismail-Beigi, S.; Louie, S. G. Excited-State Forces within a First-Principles Green's Function Formalism. *Phys. Rev. Lett.* **2003**, *90*, No. 076401.
(63) Hohenberg, P.; Kohn, W. Inhomogeneous Electron Gas. *Phys. Rev.* **1964**, *136*, B864−B871.
(64) Kohn, W.; Sham, L. J. Self-Consistent Equations Including Exchange and Correlation Effects. *Phys. Rev.* **1965**, *140*, A1133−A1138.
(65) Parr, R. G.; Yang, W. *Density-Functional Theory of Atoms and Molecules*; Clarendon Press: Oxford, 1989.
(66) Olsen, T.; Thygesen, K. S. Static Correlation Beyond the Random Phase Approximation: Dissociating H_2 With the Bethe-Salpeter Equation and Time-Dependent GW. *J. Chem. Phys.* **2014**, *140*, 164116.
(67) Holzer, C.; Gui, X.; Harding, M. E.; Kresse, G.; Helgaker, T.; Klopper, W. Bethe−Salpeter Correlation Energies of Atoms and Molecules. *J. Chem. Phys.* **2018**, *149*, 144106.
(68) Li, J.; Drummond, N. D.; Schuck, P.; Olevano, V. Comparing Many-Body Approaches Against the Helium Atom Exact Solution. *SciPost Phys.* **2019**, *6*, No. 040.
(69) Li, J.; Duchemin, I.; Blase, X.; Olevano, V. Ground-State Correlation Energy of Beryllium Dimer by the Bethe−Salpeter Equation. *SciPost Phys.* **2020**, *8*, No. 020.
(70) Harding, M. E.; Vazquez, J.; Ruscic, B.; Wilson, A. K.; Gauss, J.; Stanton, J. F. High-Accuracy Extrapolated ab Initio Thermochemistry. III. Additional Improvements and Overview. *J. Chem. Phys.* **2008**, *128*, 114111.
(71) Furche, F.; Van Voorhis, T. Fluctuation-Dissipation Theorem Density-Functional Theory. *J. Chem. Phys.* **2005**, *122*, 164106.
(72) Maggio, E.; Kresse, G. Correlation energy for the homogeneous electron gas: Exact Bethe-Salpeter solution and an approximate evaluation. *Phys. Rev. B: Condens. Matter Mater. Phys.* **2016**, *93*, 235113.
(73) Furche, F. Developing the Random Phase Approximation Into a Practical Post-Kohn−Sham Correlation Model. *J. Chem. Phys.* **2008**, *129*, 114105.
(74) Toulouse, J.; Gerber, I. C.; Jansen, G.; Savin, A.; Angyan, J. G. Adiabatic-Connection Fluctuation-Dissipation Density-Functional Theory Based on Range Separation. *Phys. Rev. Lett.* **2009**, *102*, No. 096404.
(75) Toulouse, J.; Zhu, W.; Angyan, J. G.; Savin, A. Range-Separated Density-Functional Theory With the Random-Phase Approximation: Detailed Formalism and Illustrative Applications. *Phys. Rev. A: At., Mol., Opt. Phys.* **2010**, *82*, No. 032502.
(76) Angyan, J. G.; Liu, R.-F.; Toulouse, J.; Jansen, G. Correlation Energy Expressions from the Adiabatic-Connection Fluctuation Dissipation Theorem Approach. *J. Chem. Theory Comput.* **2011**, *7*, 3116−3130.
(77) Ren, X.; Rinke, P.; Joas, C.; Scheffler, M. Random-Phase Approximation and Its Applications in Computational Chemistry and Materials Science. *J. Mater. Sci.* **2012**, *47*, 7447−7471.
(78) van Setten, M. J.; Caruso, F.; Sharifzadeh, S.; Ren, X.; Scheffler, M.; Liu, F.; Lischner, J.; Lin, L.; Deslippe, J. R.; Louie, S. G.; Yang, C.; Weigend, F.; Neaton, J. B.; Evers, F.; Rinke, P. *GW* 100: Benchmarking G_0W_0 for Molecular Systems. *J. Chem. Theory Comput.* **2015**, *11*, 5665−5687.
(79) Maggio, E.; Liu, P.; van Setten, M. J.; Kresse, G. *GW* 100: A Plane Wave Perspective for Small Molecules. *J. Chem. Theory Comput.* **2017**, *13*, 635−648.
(80) Loos, P. F.; Romaniello, P.; Berger, J. A. Green Functions and Self-Consistency: Insights From the Spherium Model. *J. Chem. Theory Comput.* **2018**, *14*, 3071−3082.
(81) Veril, M.; Romaniello, P.; Berger, J. A.; Loos, P. F. Unphysical Discontinuities in GW Methods. *J. Chem. Theory Comput.* **2018**, *14*, 5220.
(82) Duchemin, I.; Blase, X. Robust Analytic Continuation Approach to Many-Body GW Calculations. *J. Chem. Theory Comput.* **2020**, *16*, 1742.
(83) Martin, R. M.; Reining, L.; Ceperley, D. M. *Interacting Electrons: Theory and Computational Approaches*; Cambridge University Press, 2016.
(84) Hedin, L. New Method for Calculating the One-Particle Green's Function with Application to the Electron-Gas Problem. *Phys. Rev.* **1965**, *139*, A796.
(85) Aryasetiawan, F.; Gunnarsson, O. The GW Method. *Rep. Prog. Phys.* **1998**, *61*, 237−312.
(86) Onida, G.; Reining, L.; Rubio, A. Electronic Excitations: Density-Functional Versus Many-Body Green's Function Approaches. *Rev. Mod. Phys.* **2002**, *74*, 601−659.
(87) Reining, L. The GW Approximation: Content, Successes and Limitations: The GW Approximation. *Wiley Interdiscip. Rev.: Comput. Mol. Sci.* **2018**, *8*, e1344.
(88) Hanke, W.; Sham, L. J. Many-Particle Effects in the Optical Spectrum of a Semiconductor. *Phys. Rev. B: Condens. Matter Mater. Phys.* **1980**, *21*, 4656.
(89) Strinati, G. Effects of Dynamical Screening on Resonances at Inner-Shell Thresholds in Semiconductors. *Phys. Rev. B: Condens. Matter Mater. Phys.* **1984**, *29*, 5718.
(90) Strinati, G. Dynamical Shift and Broadening of Core Excitons in Semiconductors. *Phys. Rev. Lett.* **1982**, *49*, 1519.

https://dx.doi.org/10.1021/acs.jpclett.0c00460
J. Phys. Chem. Lett. 2020, 11, 3536−3545

(91) Dreuw, A.; Head-Gordon, M. Single-Reference Ab Initio Methods for the Calculation of Excited States of Large Molecules. *Chem. Rev.* **2005**, *105*, 4009−4037.
(92) Holzer, C.; Teale, A. M.; Hampe, F.; Stopkowicz, S.; Helgaker, T.; Klopper, W. GW Quasiparticle Energies of Atoms in Strong Magnetic Fields. *J. Chem. Phys.* **2019**, *150*, 214112.
(93) Colonna, N.; Hellgren, M.; de Gironcoli, S. Correlation Energy Within Exact-Exchange Adiabatic Connection Fluctuation-Dissipation Theory: Systematic Development and Simple Approximations. *Phys. Rev. B: Condens. Matter Mater. Phys.* **2014**, *90*, 125150.
(94) Hybertsen, M. S.; Louie, S. G. First-Principles Theory of Quasiparticles: Calculation of Band Gaps in Semiconductors and Insulators. *Phys. Rev. Lett.* **1985**, *55*, 1418−1421.
(95) Christiansen, O.; Koch, H.; Jørgensen, P. The Second-Order Approximate Coupled Cluster Singles and Doubles Model CC2. *Chem. Phys. Lett.* **1995**, *243*, 409−418.
(96) Purvis, G. P., III; Bartlett, R. J. A Full Coupled-Cluster Singles and Doubles Model: The Inclusion of Disconnected Triples. *J. Chem. Phys.* **1982**, *76*, 1910−1918.
(97) Christiansen, O.; Koch, H.; Jørgensen, P. Response Functions in the CC3 Iterative Triple Excitation Model. *J. Chem. Phys.* **1995**, *103*, 7429−7441.
(98) Aidas, K.; et al. The Dalton Quantum Chemistry Program System. *WIREs Comput. Mol. Sci.* **2014**, *4*, 269−284.
(99) Parrish, R. M.; Burns, L. A.; Smith, D. G. A.; Simmonett, A. C.; DePrince, A. E.; Hohenstein, E. G.; Bozkaya, U.; Sokolov, A. Y.; Di Remigio, R.; Richard, R. M.; Gonthier, J. F.; James, A. M.; McAlexander, H. R.; Kumar, A.; Saitow, M.; Wang, X.; Pritchard, B. P.; Verma, P.; Schaefer, H. F.; Patkowski, K.; King, R. A.; Valeev, E. F.; Evangelista, F. A.; Turney, J. M.; Crawford, T. D.; Sherrill, C. D. Psi4 1.1: An Open-Source Electronic Structure Program Emphasizing Automation, Advanced Libraries, and Interoperability. *J. Chem. Theory Comput.* **2017**, *13*, 3185−3197 PMID: 28489372..
(100) Hättig, C.. Structure Optimizations for Excited States with Correlated Second-Order Methods: CC2 and ADC(2). In *Response Theory and Molecular Properties (A Tribute to Jan Linderberg and Poul Jørgensen)*; Jensen, H. A., Ed.; Advances in Quantum Chemistry; Academic Press, 2005; Vol. *50*; pp 37−60.
(101) Budzák, Š.; Scalmani, G.; Jacquemin, D. Accurate Excited-State Geometries: a CASPT2 and Coupled-Cluster Reference Database for Small Molecules. *J. Chem. Theory Comput.* **2017**, *13*, 6237−6252.
(102) Kállay, M.; Rolik, Z.; Csontos, J.; Nagy, P.; Samu, G.; Mester, D.; Csóka, J.; Szabó, B.; Ladjánszki, I.; Szegedy, L.; Ladóczki, B.; Petrov, K.; Farkas, M.; Mezei, P. D.; Hégely, B. *MRCC, Quantum Chemical Program*; 2017.
(103) Duchemin, I.; Blase, X. Separable Resolution-of-the-Identity with All-Electron Gaussian Bases: Application to Cubic-scaling RPA. *J. Chem. Phys.* **2019**, *150*, 174120.
(104) Garniron, Y.; Gasperich, K.; Applencourt, T.; Benali, A.; Ferté, A.; Paquier, J.; Pradines, B.; Assaraf, R.; Reinhardt, P.; Toulouse, J.; Barbaresco, P.; Renon, N.; David, G.; Malrieu, J. P.; Véril, M.; Caffarel, M.; Loos, P. F.; Giner, E.; Scemama, A. Quantum Package 2.0: A Open-Source Determinant-Driven Suite Of Programs. *J. Chem. Theory Comput.* **2019**, *15*, 3591.
(105) Scemama, A.; Garniron, Y.; Caffarel, M.; Loos, P. F. Deterministic Construction of Nodal Surfaces Within Quantum Monte Carlo: The Case of FeS. *J. Chem. Theory Comput.* **2018**, *14*, 1395.
(106) Caruso, F.; Rohr, D. R.; Hellgren, M.; Ren, X.; Rinke, P.; Rubio, A.; Scheffler, M. Bond Breaking and Bond Formation: How Electron Correlation Is Captured in Many-Body Perturbation Theory and Density-Functional Theory. *Phys. Rev. Lett.* **2013**, *110*, 146403.
(107) Hellgren, M.; Caruso, F.; Rohr, D. R.; Ren, X.; Rubio, A.; Scheffler, M.; Rinke, P. Static Correlation and Electron Localization in Molecular Dimers from the Self-Consistent RPA and G W Approximation. *Phys. Rev. B: Condens. Matter Mater. Phys.* **2015**, *91*, 165110.

https://dx.doi.org/10.1021/acs.jpclett.0c00460
J. Phys. Chem. Lett. 2020, 11, 3536−3545